

The Statistics of the Cross-Spectrum and the Spectrum Average: Generalization to Multiple Instruments

Antoine Baudiquez^{ID}, *Graduate Student Member, IEEE*, Éric Lantz^{ID},
 Enrico Rubiola^{ID}, *Member, IEEE*, and François Vernotte^{ID}

Abstract—This article addresses the measurement of the power spectrum of red noise processes at the lowest frequencies, where the minimum acquisition time is so long that it is impossible to average on a sequence of data record. Therefore, averaging is possible only on simultaneous observation of multiple instruments. This is the case of radio astronomy, which we take as the paradigm, but examples may be found in other fields such as climatology and geodesy. We compare the Bayesian confidence interval of the red noise parameter using two estimators, the spectrum average and the cross-spectrum. While the spectrum average is widely used, the cross-spectrum using multiple instruments is rather uncommon. With two instruments, the cross-spectrum estimator leads to the Variance–Gamma distribution. A generalization to q devices based on the Fourier transform of characteristic functions is provided, with the example of the observation of millisecond pulsars with five radio telescopes (RTs). The simulations show that the spectrum average is by a small amount more efficient than the cross-spectrum, chiefly when the background exceeds the signal. However, some notable differences between their upper limit indicate that it should be wiser to compute both estimators.

Index Terms—Bayesian statistics, characteristic function, confidence interval, cross-spectrum, Karhunen-Loève transform (KLT), Monte Carlo simulation, probability density function, QR decomposition, spectrum average.

I. INTRODUCTION

THE term red noise refers to a variety of processes sharing the property that the power spectral density (PSD) grows

Manuscript received 14 March 2022; accepted 20 June 2022. Date of publication 22 June 2022; date of current version 29 July 2022. This work was supported in part by the Agence Nationale de la Recherche (ANR) Programs d'Investissement d'Avenir (PIA) Oscillateur Instabilité Measurement Platform (IMP) under Project 11-EQPX-0033 and in part by FIRST-TF under Project 10-LABX-0048. (*Corresponding author: Antoine Baudiquez.*)

Antoine Baudiquez is with the Department of Time and Frequency, FEMTO-ST, UMR 6174, Université Bourgogne Franche-Comté, 25030 Besançon, France (e-mail: antoine.baudiquez@femto-st.fr).

Éric Lantz is with the Département d'Optique P.M. Duffieux, FEMTO-ST, UMR 6174 CNRS, Université Bourgogne Franche-Comté, 25030 Besançon, France.

Enrico Rubiola is with the Department of Time and Frequency, FEMTO-ST, UMR 6174 CNRS, Université Bourgogne Franche-Comté, 25030 Besançon, France, and also with the Physics Metrology Division, Istituto Nazionale di Ricerca Metrologica (INRiM), 10135 Turin, Italy.

François Vernotte is with the Department of Time and Frequency, FEMTO-ST, Observatory THETA, UMR 6174 CNRS, Université Bourgogne Franche-Comté, 25030 Besançon, France.

Digital Object Identifier 10.1109/TUFFC.2022.3185528

at low frequency as $1/f^2$ (Brownian noise) or $1/f^\alpha$, with $\alpha > 2$. We are interested in the estimation of the PSD of such random signals out of the background noise of the instrument in the specific case of very slow phenomena, which take too long acquisition time for the average on a sequence of datasets to be viable. Therefore, averaging out the background is possible only by exploiting simultaneous measurements of the same signal taken with multiple instruments, under the obvious hypothesis that they are independent. The frequency stability of the millisecond pulsars is the example we have in mind. Such rapidly rotating neutron stars, emitting highly stable periodic pulses out of the magnetic poles, rival the best atomic clocks [1]–[4]. Among other fields, slow phenomena are found in climatology [5] and geodesy, the latter nowadays measured with Very Large Baseline Interferometry [6]. The measurement of noise and phase noise with fully digital instruments is another appealing application because increasing the number of channels is reasonably simple. The phase noise of oscillators can be measured with the multi-channel tracking DDS [7]. An improved 16-channel version of the Tracking DDS is now a semi-commercial instrument (we have recently purchased two beta-test samples), albeit there is still no official announcement. In Si, Ge, and GaAs semiconductors, low $1/f$ noise is a quality indicator related to the effective number of defects [8].

With the purposes stated in mind, we compare the efficiency of the spectrum average (s.a) and with the cross-spectrum (c-s) measuring the signal with q instruments simultaneously. The s.a estimator is the average of the q observed spectra S_i , weighted with the background noise $\sigma_{N,i}^2$ of the i th instrument. The c-s method is the average of the all combinatorial choices of the cross-spectrum $S_{j,i}$, $i \neq j$. The s.a is the classical estimator used in these cases [9], while the c-s is rather uncommon. Data are analyzed with the Bayesian statistics, also known as the inverse problem, which consists of estimating the most probable value of the signal (the slowest spectral components) from the experimental outcomes and their statistical properties. We take the 95% upper limit as the efficiency criterion. Accordingly, the most efficient estimator is the one that provides the most stringent upper limit on the variance of the signal with the same dataset.

Our previous article [10] shows that the Variance–Gamma (VG) distribution is the exact solution for the probability density function (PDF) of the cross-spectrum in the case of

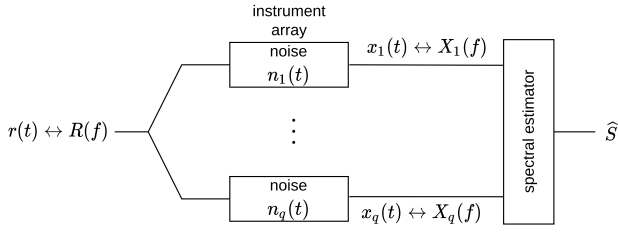


Fig. 1. Array of q instruments measuring the signal $r(t)$. Each instrument adds a white noise to the output $x(t)$ whose Fourier transform is $X(f)$. Then the estimate \hat{S} is computed.

two instruments. We generalize the result to the case of the cross-spectrum of q instruments, each with its own background noise $\sigma_{N_i}^2$, assessing the confidence interval on the signal-level σ_R^2 . Of course, the PDF is no longer a $V\Gamma$, and can only be calculated numerically. The case of equally noisy instruments is simpler, and at first sight similar to that of $q = 2$, but it has no analytical solution.

We run a simulation with up to five instruments, inspired to the LEAP experiment [11]. Such experiment gathers the five largest European radio telescopes (RTs) to increase the sensitivity of high-precision pulsar timing. Interestingly, pulsar timing arrays seem a promising option to explore the low-frequency gravity waves crossing our Galaxy [12], [13]. The c-s estimator commonly used in the frequency metrology has recently been used in [14] to show the detection limit of correlated red noise. Hence defining a confidence interval on this estimator and comparing it with the commonly used s.a will give hints on which estimator has to be privileged to improve the sensitivity.

This article is intended to compare the s.a and the c-s estimators generalized to multiple instruments measuring a random signal, e.g., a red noise. In this respect, we define both estimators of the PSD and describe their statistical properties in Section II. Then in Section III we give their probability density function. Sections IV and V compare the confidence interval of the red noise respectively between the s.a and the Karhunen–Loève transform (KLT), and between the s.a and the c-s. Conclusions are presented in Section VI.

II. TWO ESTIMATORS OF THE PSD

A. Spectral Measurement

Let us consider a red noise $r(t)$ which is measured by q independent instruments as shown in Fig. 1. We assume that each instrument adds a white noise $n_i(t)$ to the measurement and that all these white noises are uncorrelated. In the following, we call the red noise the “signal” and the white noise from the measurement instrument is referred as the “measurement noise.” The output of each channel is then:

$$x_i = r + n_i \leftrightarrow X_i = R + N_i \quad (1)$$

where the subscript i corresponds to the i th instrument, \leftrightarrow stands for the Fourier transform and inverse Fourier transform pair, lower case is time domain, upper case is frequency domain, and the variables t and f are implied. Let us remind that the Fourier transform of a white noise is a white noise,

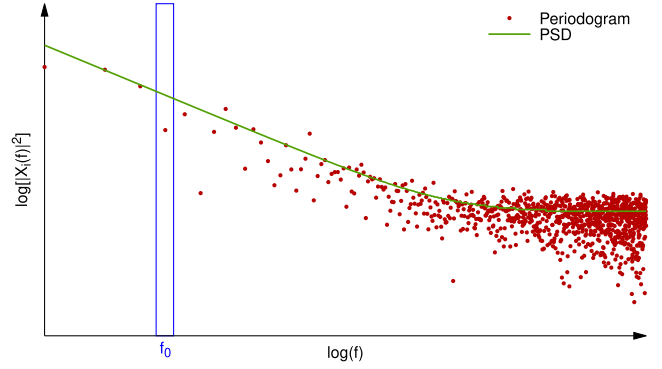


Fig. 2. Periodogram of x (white noise plus red noise). The PSD is the expectation of the periodogram.

at least for sampled signals. Indeed, even if continuous pure white noise have an infinite power, the Fourier transform for discrete simulation can be defined. A realistic white noise corresponds to a Markov process of the first order; more details about colored noise are given in [15].

On the other hand, a red noise can be described as a filtered white noise. Its spectrum is then the product of a white spectrum by a deterministic function; so the random part of a red noise is uncorrelated for each frequency bin. Consequently, in term of random variable, working in the frequency domain gives a precious advantage because the Fourier components (frequency bins) are statistically independent unlike the time data.

In the following we focus solely on one frequency bin, thanks to energy equipartition it follows:

$$\begin{aligned} \mathbb{V}[N_i] &= 2\mathbb{V}[\Re[N_i]] = 2\mathbb{V}[\Im[N_i]] = \sigma_{N_i}^2 \\ \mathbb{V}[R] &= 2\mathbb{V}[\Re[R]] = 2\mathbb{V}[\Im[R]] = \sigma_R^2 \end{aligned} \quad (2)$$

where $\mathbb{V}[\cdot]$, $\Re[\cdot]$, and $\Im[\cdot]$ respectively denote the variance, the real, and imaginary parts of the quantity within the brackets.

B. Periodogram and Power Spectral Density

First, let us recall some basics of frequency analysis. Using a data record of duration T sampled at a suitable frequency, the periodogram is

$$P_x(f) = \frac{2}{T} |X(f)|^2, \quad f > 0 \quad (3)$$

where the factor “2” is needed for energy conservation after deleting the negative frequencies. The expectation of the periodogram is the PSD

$$S_x(f) = \mathbb{E} \left[\frac{2}{T} |X(f)|^2 \right], \quad f > 0. \quad (4)$$

Fig. 2 shows the periodogram and the PSD. We estimate the PSD as the average periodogram, with the ultimate goal of expecting the red noise parameters of r out of the measurement noise n . Of course, r is the same for all instruments, while the n_i are specific to the i th instrument and its environment.

The total duration of the experiment is the major problem, as the lowest frequency of interest sets T . In turn, a long

T goes with a small number p of averages because the total duration of the experiment is pT . In this article, we focus on the slowest red noise phenomena, up to years, for which we have to set $p = 1$. In other words, the phenomena of interest are so slow that we cannot average on multiple acquisitions.

C. Estimators

We are now focusing on one bin of the periodogram of a single simultaneous measurement with q instruments, e.g., f_0 as represented on Fig. 2. Let us emphasize on the term periodogram which designates a unique realization of the red noise since all instruments observe this red noise realization at the same time. Nevertheless, taking into account the uncorrelated white noises coming from the instruments, we have to deal with the PSD S . One bin of S represents the power in a given bandwidth, i.e. the 2nd central moment, or variance. Hereinafter, we work on a generic bin, thus $S(f)$ at that frequency is replaced with σ^2 .

Because the N_i are all different, it is appropriate to use a weighted average, where the weights α_i are to be found for the optimum detection of R . We denote the estimates with a ‘‘hat,’’ then

$$\hat{\mu} = \frac{\sum_i^q \alpha_i X_i}{\sum_i^q \alpha_i} \quad (5)$$

where q is the number of instruments. The variance of the estimate $\hat{\mu}$ is

$$\mathbb{V}[\hat{\mu}] = \frac{\sum_i^q \alpha_i^2 (\sigma_{N,i}^2 + \sigma_R^2)}{[\sum_i^q \alpha_i]^2}. \quad (6)$$

An optimal choice is obtained by solving

$$\frac{\partial \mathbb{V}[\hat{\mu}]}{\partial \alpha_i} = 0 \quad (7)$$

which leads to the solution

$$\alpha_i = \frac{1}{\sigma_{N,i}^2}. \quad (8)$$

Therefore, the inverse-variance weighted average, described in [16] with applications examples, has the least variance among all weighted averages. Then (6) becomes

$$\sigma_\mu^2 = \mathbb{V}[\hat{\mu}] = \left(\sum_i^q \frac{1}{\sigma_{N,i}^2} \right)^{-1}. \quad (9)$$

Let us define now the two estimators of interest: the spectrum average weighted by the noise variance $\sigma_{N,i}^2$ and the cross-spectrum

$$\begin{aligned} \widehat{S}_{sa} &= \left\{ \Re \left[\sigma_\mu^2 \sum_i^q \frac{X_i}{\sigma_{N,i}^2} \right] \right\}^2 + \left\{ \Im \left[\sigma_\mu^2 \sum_i^q \frac{X_i}{\sigma_{N,i}^2} \right] \right\}^2 \\ \widehat{S}_{cs} &= \langle \Re[X_i \cdot \tilde{X}_j] \rangle_m \quad \text{with } i \neq j. \end{aligned} \quad (10)$$

Moreover σ_μ^2 corresponds to the noise weight normalization factor defined in (9). Finally, $\langle \cdot \rangle$ stands for the m average over the different combinations of instruments with $m = \binom{q}{2}$ and $\tilde{\cdot}$ stands for the complex conjugate of the quantity which is below. For better readability, we have omitted in (10) a factor

$2/T$, where T is the measurement time (acquisition of the data record for one FFT), necessary for $S(f)$ to have the dimension of a PSD, and the factor fix the total power after deleting the negative frequencies. In addition, only the random part has a direct influence on the probability density function. Denoting $\mathbb{E}[\cdot]$ the mathematical expectation of the quantity within the brackets

$$\begin{cases} \mathbb{E}[\widehat{S}_{sa}] = \sigma_R^2 + \sigma_\mu^2 \\ \mathbb{E}[\widehat{S}_{cs}] = \sigma_R^2 \end{cases} \quad (11)$$

which means that the spectrum average estimator is biased. Usually, one removes the bias to have the s.a estimate average over realizations which tends toward the sought signal-level σ_R^2 . This gives a clear advantage to the c-s estimator. However, we will see that the computation of the confidence interval over the signal-level σ_R^2 requires an estimation of this bias σ_μ^2 whatever the chosen estimator, s.a or c-s. Therefore, we want to estimate the PSD and we assume it follows a $1/f^\alpha$ power law, then we only have to estimate a level and exponent of the first frequency bins.

We now compare the estimator defined in (10) by determining their variance. We can demonstrate provided that $\forall i, \sigma_{N,i}^2 = \sigma_N^2$ (see Annex)

$$\mathbb{V}[\widehat{S}_{cs}] \approx \begin{cases} \mathbb{V}[\widehat{S}_{sa}], & \text{if } \sigma_R^2 \gg \sigma_N^2 \\ \frac{q}{q-1} \mathbb{V}[\widehat{S}_{sa}], & \text{if } \sigma_R^2 \ll \sigma_N^2. \end{cases} \quad (12)$$

This is confirmed by Fig. 3 which exhibits the variance of the estimates of both estimators applied to a signal composed of a mixture of uncorrelated white noise of level 1 arbitrary unit (a.u.) and a common f^{-4} noise of level 4096 a.u. for two instruments. Therefore, the variance decreases in f^{-8} and Fig. 3 compares these variances to the square of the PSD. At $f = 4$ a.u., the signal PSD is 16 times higher than the white level and therefore its square is 256 times higher. In this case, the variances of both estimators coincide. On the other hand, for frequencies higher than 16 a.u., the signal PSD is less than 16 times lower than the white level (256 for their squares) and the variance of the c-s estimates is two times higher than the variance of the s.a estimates. This seems to indicate a better efficiency of the s.a estimator. Indeed, the spectrum average estimator is a sufficient estimator which means of minimal variance.

However what about the PDF of the estimates knowing the parameter σ_R^2 for a given frequency?

III. PROBABILITY DENSITY FUNCTION

A. Spectrum Average Method

The spectrum average estimator leads to the following χ^2 distribution with two degrees of freedom resulting from the real and imaginary parts of the spectrum:

$$p(\widehat{S}_{sa} | \sigma_R^2) = \frac{e^{-\frac{\widehat{S}_{sa}}{2\sigma^2}}}{2\sigma^2} \quad (13)$$

where

$$\sigma^2 = \frac{1}{2}(\sigma_\mu^2 + \sigma_R^2) \quad (14)$$

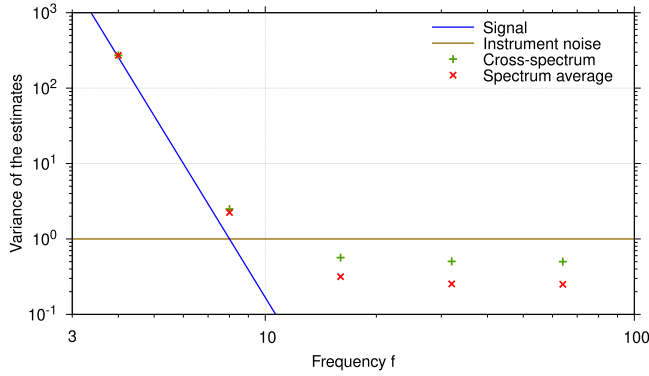


Fig. 3. Variance of the estimate with the signal variance which is of the form $(\sigma_R^2/f^\alpha)^2$, where $\sigma_R^2 = 4096$ a.u. is the signal level and $\alpha = 4$ the red noise exponent. The noise model is a white noise of level $\sigma_N^2 = 1$ a.u. with two instruments.

where σ_μ^2 is the weighted noise level according to (9) and σ_R^2 the signal level of interest.

B. Karhunen-Loève Transform

The KLT method, denoting to the KLT, has been developed in [17]. It uses the statistics of the data themselves instead of the statistics of the estimates. This method has the advantage to combine linearly independent Gaussian estimates. Furthermore, it also forms a sufficient statistics like the s.a method. It is based on determining the covariance matrix M associated with the real or imaginary part of the measurement X_i obtained by the q instruments

$$\begin{cases} M_{ii} = \frac{1}{2}(\sigma_{N,i}^2 + \sigma_R^2) \\ M_{ij} = \frac{1}{2}\sigma_R^2, \quad \text{with } i \neq j \end{cases} \quad (15)$$

where the extra factors $1/2$ come from (2). This covariance matrix has to be diagonalized and we denote the eigenvalues λ_i . Their associated normalized eigenvectors are V_i and the PDF is then given by

$$p(\widehat{S_{\text{KLT}}}| \sigma_R^2) = \prod_{i=1}^q \frac{1}{(2\pi \lambda_i)^{\nu/2}} e^{-\frac{\sum_{j=1}^{\nu} w_{ij}^2}{2\lambda_i}} \quad (16)$$

where j highlights the real and imaginary part obtained through the Fourier transform therefore $\nu = 2$. Let us remind that X corresponds to the matrix containing the set of Fourier transform of the measurements at the output of each instrument. The numerator of the exponential argument is then

$$w = X \cdot V \quad (17)$$

where V are the eigenvectors obtained from the diagonalized covariance matrix.

C. Cross-Spectrum

The cross-spectrum estimator leads to the variance-gamma (VG) distribution for two instruments as described in Section III in [10] but for more than two instruments it is no longer the case. Having no exact solution known nowadays,

we propose a solution based on the characteristic function. Expanding the model from the case of two instruments, we define a basis such as in [10]

$$\mathcal{B} = \begin{pmatrix} \sigma_{N,1}/2 & \sigma_{N,1}/2 & \dots & \dots & \sigma_{N,1}/2 \\ \sigma_{N,2}/2 & -\sigma_{N,2}/2 & 0 & \dots & 0 \\ 0 & 0 & -\sigma_{N,3}/2 & \dots & 0 \\ \vdots & \vdots & \vdots & \ddots & -\sigma_{N,q}/2 \\ \sigma_R & 0 & 0 & \dots & 0 \end{pmatrix}. \quad (18)$$

We apply the DGEQRF LAPACK subroutine on \mathcal{B} . The outputs enable the computation of the product of elementary reflectors which is a matrix $\mathcal{Q}(q+1, q+1)$. Then we define \mathcal{W} the matrix where each column contains the standard deviation of the spectrum according to (1) as

$$\mathcal{W} = \frac{1}{\sqrt{2}} \begin{pmatrix} \sigma_{N,1} & 0 & \dots & \dots & 0 \\ 0 & \sigma_{N,2} & 0 & \dots & 0 \\ 0 & 0 & \sigma_{N,3} & \dots & 0 \\ \vdots & \vdots & \vdots & \ddots & \sigma_{N,q} \\ \sigma_R & \sigma_R & \sigma_R & \dots & \sigma_R \end{pmatrix}. \quad (19)$$

All the measurement noises are independent, as assumed, whereas the signal is common. Then the columns of \mathcal{W} are projected onto the orthogonal basis \mathcal{Q} and each pair of cross-spectra according to (10) is determined. Finally, we compute the eigenvalues λ_j of the resulting components using the DSYEV LAPACK subroutine. This leads to a linear combination of χ^2 distribution as follows:

$$\widehat{S_{\text{cs}}} = \sum_j^q \lambda_j \chi_k^2 \quad (20)$$

where k is the number of degrees of freedom corresponding to each eigenvalue, e.g., equal to 2 for the real and imaginary parts without degeneration. In the special case of two instruments, we obtain the subtraction of two χ^2 random variables with the same number of degrees of freedom. The characteristic function of the χ_k^2 distribution is defined as

$$\phi_j(t) = (1 - 2i\lambda_j t)^{-k/2} \quad (21)$$

where i is the imaginary unit and we apply a variable change of $-t$ for the negative eigenvalues. The χ^2 distributions according to (20) being independent, the characteristic function of the c-s becomes

$$\phi(t) = \prod_j^q \phi_j(t). \quad (22)$$

It leads to the moment generating function of the VG distribution for two instruments but it is no longer the case for more instruments. When all the instruments have the same level of intrinsic noise σ_n^2 , the diagonalization of the matrix \mathcal{W} defined by (19) leads to two eigenvalues. One is unique and the second one has a degeneration of $q - 1$ with q the number of instruments. Consequently, it leads to the difference of two χ^2 random variables with different degrees of freedom. However, even if it looks like the case with two instruments, the difference in the degrees of freedom of the χ^2 distributions

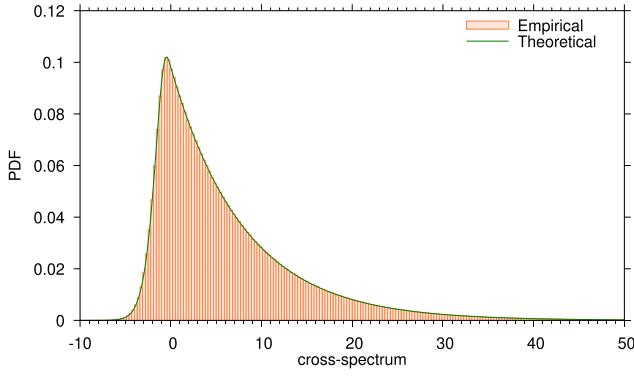


Fig. 4. Comparison of the empirical (red boxes) and theoretical (green line) PDF of the c-s for five instruments where the variances are $\sigma_R^2 = 6$ a.u. and $\sigma_N^2 = 10$ a.u.

has no analytical solution. Therefore, the probability density function of the c-s for any noise level is defined as

$$p(\widehat{S}_{cs} | \sigma_R^2) = \frac{1}{2\pi} \int_{\mathbb{R}} e^{-it\widehat{S}_{cs}} \phi(t) dt. \quad (23)$$

We perform the integration of the real part of the function using the Simpson method only on the positive reals because the real part of this function is even whereas the imaginary part is odd. Fig. 4 shows that the theoretical probability density function fits very well the histogram obtained by 10^7 Monte Carlo simulations for 5 instruments. The variance of each white noise is the same $\sigma_N^2 = 10$ a.u. whereas the signal level is $\sigma_R^2 = 6$ a.u.

D. Bayesian Inference

1) *Posteriori Distribution*: We seek to determine a confidence interval on σ_R^2 , but (13), (16) and (23) define the PDF of a set of measurement X given the sought parameter σ_R^2 . So we have to solve the inverse problem which means to determine the PDF of σ_R^2 given a set of measurement X called the *posterior* distribution. The Bayes theorem leads to the following relation:

$$\begin{cases} p(\sigma_R^2 | X) \propto p(X | \sigma_R^2) \cdot \pi(\sigma_R^2) \\ \int_0^\infty p(\sigma_R^2 | X) d\sigma_R^2 = 1 \end{cases} \quad (24)$$

where $\pi(\sigma_R^2)$ is the prior, i.e., the PDF before any measurement. One of the main issue of Bayesian analysis concerns the choice of this prior.

2) *Choice of the Prior*: To be as general as possible, we will assume a total ignorance of the signal level. In such a case, it is generally considered that any order of magnitude has the same probability which suggests a constant prior in a logarithmic scale, i.e., $\pi(\sigma_R^2) = 1/\sigma_R^2$. However, our perfect knowledge of the measurement noise level induces an implicit scale factor. In other words, since we did not remove the ‘‘bias’’ σ_μ^2 in (11), the s.a estimator is shifted by σ_μ^2 . In a very similar case [18], we decided that the true parameter should be the sum of both levels $\theta = \sigma_\mu^2 + \sigma_R^2$. Moreover according to (9) higher noise will have lower weight and in our case, since the mathematical

expectation of the s.a estimator is $\sigma_\mu^2 + \sigma_R^2$, it comes naturally that the true parameter should be

$$\theta = \sigma_\mu^2 + \sigma_R^2. \quad (25)$$

From these considerations, we will choose $\pi(\theta) = 1/\theta = (1/(\sigma_\mu^2 + \sigma_R^2))$ and then, our prior for the s.a estimator will be

$$\pi(\sigma_R^2) \propto \frac{1}{\sigma_\mu^2 + \sigma_R^2}. \quad (26)$$

To be fair in the trial of c-s against s.a, the same prior will be used for both estimators.

In the following we will compare the different methods, starting with the spectrum average and KLT in Section IV.

IV. SPECTRUM AVERAGE AND KLT COMPARISON

A. Particular Case: all the Instruments Have the Same Variance

Let us define $\forall i, \sigma_{N,i}^2 = \sigma_N^2$, i.e., all the q instruments have the same noise level. At a first step we determine the s.a PDF, in this case according to (9) and (2), the variance defined by (14) leads to the following expression:

$$\sigma^2 = \frac{1}{2} \left(\frac{\sigma_N^2}{q} + \sigma_R^2 \right). \quad (27)$$

From (10), the estimate \widehat{S}_{sa} now becomes

$$\begin{aligned} \widehat{S}_{sa} &= \left\{ \Re \left[\sigma_\mu^2 \sum_i^q \frac{X_i}{\sigma_{N,i}^2} \right] \right\}^2 + \left\{ \Im \left[\sigma_\mu^2 \sum_i^q \frac{X_i}{\sigma_{N,i}^2} \right] \right\}^2 \\ &= \frac{1}{q^2} \left(\left\{ \Re \left[\sum_i^q X_i \right] \right\}^2 + \left\{ \Im \left[\sum_i^q X_i \right] \right\}^2 \right). \end{aligned} \quad (28)$$

According to (13), the s.a PDF is given by

$$p(\widehat{S}_{sa} | \sigma_R^2) = \frac{e^{-\frac{1}{2\sigma^2} [\Re[\sum_i^q x_i]^2 + \Im[\sum_i^q x_i]^2]}}{\frac{\sigma_N^2 + \sigma_R^2}{q}}. \quad (29)$$

In a second step let us define the KLT PDF. The eigenvalues of the covariance matrix resulting from (15) are given by

$$\begin{aligned} \lambda_1 &= \frac{1}{2} (\sigma_N^2 + q\sigma_R^2) \\ \lambda_i &= \frac{1}{2} \sigma_N^2, \quad \text{with } i \in \{2, \dots, q\}. \end{aligned} \quad (30)$$

The first and highest eigenvalue being the only one to depend of σ_R^2 , we solely define its associated eigenvector

$$V_1 = \frac{J_{q,1}}{\sqrt{q}} \quad (31)$$

where $J_{q,1}$ is the all-ones column vector. Then the numerator in the exponential in (16) is

$$\begin{aligned} \sum_j^v \hat{w}_{1,j}^2 &= \sum_j^v [X_j \cdot V_1]^2 \\ &= \frac{1}{q} \sum_j^v [X_j \cdot J_{q,1}]^2 \\ &= \frac{1}{q} \sum_j^v \left[\sum_i^q X_{ij} \right]^2 \\ &= \frac{1}{q} \left\{ \Re \left[\sum_i^q X_i \right]^2 + \Im \left[\sum_i^q X_i \right]^2 \right\}. \end{aligned} \quad (32)$$

The KLT PDF defined by (16) is given by

$$p(\widehat{S}_{\text{KLT}} | \sigma_R^2) = C \frac{e^{-\frac{\frac{1}{q} \left[\Re \left[\sum_i^q X_i \right]^2 + \Im \left[\sum_i^q X_i \right]^2 \right]}{\sigma_N^2 + q\sigma_R^2}}}{\pi (\sigma_N^2 + q\sigma_R^2)} \quad (33)$$

where C is the Gaussian remaining product with a variance depending only on the measurement noise level. However, what we want to characterize is not the estimates but the parameter σ_R^2 . According to (24), the PDF of the true parameter σ_R^2 is proportional to the prior $\pi(\sigma_R^2)$ multiplied respectively by (29) and (33) for the s.a and KLT estimates. The Bayes theorem leads then to

$$p(\sigma_R^2 | \widehat{S}_{\text{sa}}) \propto \pi(\sigma_R^2) \frac{e^{-\frac{\frac{1}{q} \left[\Re \left[\sum_i^q X_i \right]^2 + \Im \left[\sum_i^q X_i \right]^2 \right]}{\sigma_N^2 + q\sigma_R^2}}}{\sigma_N^2 + q\sigma_R^2} \quad (34)$$

and

$$p(\sigma_R^2 | \widehat{S}_{\text{KLT}}) \propto \pi(\sigma_R^2) \frac{e^{-\frac{\frac{1}{q} \left[\Re \left[\sum_i^q X_i \right]^2 + \Im \left[\sum_i^q X_i \right]^2 \right]}{\sigma_N^2 + q\sigma_R^2}}}{\sigma_N^2 + q\sigma_R^2}. \quad (35)$$

Multiplying respectively (34) and (35) by a factor $1/q$ and π does not change the PDF since it is normalized. It is exactly the same for (35) where C does not depend on σ_R^2 and vanish through the normalization. Therefore, both expressions are exactly the same. It should also be noted that the noise-level σ_N^2 is necessary in both cases and the bias does not influence the sought parameter density whereas it does regarding the estimates. This implies a very interesting consequence: both PDF for the s.a and KLT lead to the exact same confidence interval for the same noise level.

B. General Case

In this part any number of instruments and different noise level for each of them can be considered. In Section IV-A, we showed analytically that both methods lead to the same PDF of the signal level knowing the estimates in the event that all noise levels are the same. However when each noise level is different (30) giving the relation between the eigenvalues and the signal becomes much more complicated without degeneration. In this case, let us consider a number of instruments solely up to 5, referring as instance to the number of RTs part of the LEAP project. Then we make several empirical

TABLE I

UPPER LIMIT AVERAGE OF THE PARAMETER σ_R^2 TAKING INTO ACCOUNT 2 TO 5 RTs. THESE DATA WERE OBTAINED FROM A SET OF 1000 SIMULATED SPECTRA. THE SIGNAL AND NOISE LEVEL USED FOR THE COMPUTATION ARE $\sigma_R^2 = 1$ AND $\sigma_{N,i}^2 = i$ WHERE i IS THE INDEX OF THE RT

RTs number	Spectrum average / KLT			95% upper limit	
	Mean	Median	Std	Min	Max
2	17.44	12.88	3.10	6.30	115.32
3	16.32	11.78	2.39	5.16	91.78
4	15.66	11.10	2.95	4.54	108.82
5	14.84	10.67	2.28	4.14	86.99

comparisons by computing the upper limit at 95% for the spectrum average and KLT methods. It should be noticed that the 5% lower bound has no interest since we are more particularly interested in the case where the signal is weaker than the noise level. This bound then greatly depends on the prior and is very close to zero.

Table I gives the average over 1000 realizations of the 95% upper bound for 2 to 5 RTs. The signal and noise levels are respectively $\sigma_R^2 = 1$ a.u. and $\sigma_{N,i}^2 = i$ a.u. where i is the i th RT. Then the 2nd and 3rd RT are respectively two and three times more noisy than the first one and so forth.

First, these comparisons show as expected that the 95% bounds obtained by both estimators as in Section IV-A for the same noise variance are exactly the same.

Second, the mean and median of the 95% upper limit of the s.a and KLT estimates obtained over 1000 realizations are decreasing as the number of RTs increases. Therefore, adding a new instrument to the array, as long as we have a perfect knowledge of its noise level, necessarily contributes to lowering the upper limit and then improve the parameter estimation. The maximum value is not really significant since the tail of the distribution is very long and thin.

Finally, it should be noticed that both methods require the noise-level knowledge for the expression of the probability density function. The spectrum average method being the fastest way to compute the confidence interval is then to be privileged. Therefore, we will only compare the spectrum average method with the cross-spectrum in the next section.

V. 95% UPPER LIMIT: SPECTRUM AVERAGE VERSUS CROSS-SPECTRUM

We have set the direct problem, i.e., the statistics of the s.a or c-s knowing the signal level and noise level (which is assumed to be known), respectively in Sections III-A and III-C. Now we tackle the inverse problem from the direct problem, i.e., the statistics of the signal level knowing the s.a or c-s estimate. The Bayes theorem enables us to establish this link as described in Section III-D. The posterior distribution of the s.a and c-s are given by

$$p(\sigma_R^2 | \widehat{S}_{\text{sa}}) \propto \frac{1}{(\sigma_\mu^2 + \sigma_R^2)^2} e^{-\frac{\widehat{S}_{\text{sa}}}{\sigma_\mu^2 + \sigma_R^2}} \quad (36)$$

and

$$p(\sigma_R^2 | \widehat{S}_{\text{cs}}) \propto \frac{1}{2\pi(\sigma_\mu^2 + \sigma_R^2)} \int_{\mathbb{R}} e^{-it\widehat{S}_{\text{cs}}} \phi(t) dt \quad (37)$$

where σ_μ^2 is the noise variance weighting according to (9). Let us describe our simulation algorithm to assess the 95% upper limit.

First simulation (S_1 to S_3): simulate a set of real data from q instruments, assuming the red noise level is known (as well as, of course, the measurement noise levels).

- S_1 : Assign the number of RTs, the noise variance of each one and the sought true signal level.
- S_2 : Generate a set of spectral measurement according to (1)
- S_3 : Compute the s.a and c-s estimates, as stated in (10), which are now fixed as parameters.

Second simulation: we no longer modify the data (these are acquired measurement results) and we look for a confidence interval on the red noise, assuming the level of the measurement noise is known.

- S_4 : Define any basis and perform an orthogonalization and normalization of it using the DGEQRF subroutine from LAPACK
- S_5 : Establish, from (19), one \mathcal{W} matrix for each signal level varying from 0 to an upper limit for which (36) and (37) are close enough to zero according to the required precision.
- S_6 : Perform S_7 to S_{11} for each σ_R^2 value.
- S_7 : Project the \mathcal{W} matrix onto the orthogonal basis.
- S_8 : Compute the c-s denoted \mathcal{Z} from the result of S_6 .
- S_9 : Determine the eigenvalues of \mathcal{Z} using the DSYEV subroutine from LAPACK which has now the form of (20).
- S_{10} : Define the product of each characteristic function defined by (21).
- S_{11} : Compute the posterior distribution respectively of the s.a and c-s estimates according to (36) and (37). For the c-s, we perform a numerical integration of one signal value using the Simpson method.
- S_{12} : Normalize the s.a and c-s posterior PDF.
- S_{13} : Determine the cumulative distribution function (cdf) by integrating the s.a and c-s posterior PDF and find the 95% upper limit corresponding onto the cdf value associated with the signal level.

The loops for the different values of the signal are computed in parallel to save computing time. Let us give an example of such a process. We set the number of RTs to 5 and the variances of the signal and noise are respectively $\sigma_R^2 = 6$ a.u., $\sigma_n^2 = 10$ a.u. Then we produce two sets of random measurement with these parameters, shown in Table II. The first measurement set gives respectively $\widehat{S}_{sa,1} = 14.886$ a.u. and $\widehat{S}_{cs,1} = 13.226$ a.u. for the s.a and c-s estimates whereas the second one gives $\widehat{S}_{sa,2} = 20.730$ a.u. and $\widehat{S}_{cs,2} = 18.564$ a.u. It leads for the first set to the 95% upper limit on the signal σ_R^2 following value, 125.8 for the s.a and 127.3 for the c-s. Furthermore, the second set gives us 167.1 for the s.a and 164.8 for the c-s. These results show that either the c-s or the s.a can be the most efficient even with the same parameters, then it only depends on the measurement set. However, the difference between the 95% upper limit for both methods is relatively low.

TABLE II
MEASUREMENT SET FOR THE OUTPUTS OF EACH RT (5 IN TOTAL)
WHERE $\sigma_R^2 = 6$ a.u. AND $\sigma_N^2 = 10$ a.u.

	measurement set 1		measurement set 2	
	Real part	Imaginary part	Real part	Imaginary part
X_1	-3.8947	-1.7994	-0.1494	8.9456
X_2	-5.0950	-3.9125	-0.5275	4.4659
X_3	-2.5133	-5.5431	0.2176	5.7742
X_4	0.6433	-1.9566	1.6044	3.2146
X_5	-0.2294	-2.5738	-0.5284	0.3563

TABLE III
95% UPPER LIMIT STATISTICS FOR THE S.A (TOP), C-S (MIDDLE) AND THE RATIO OF THE S.A BY THE C-S OVER 100 SIMULATIONS WHERE $\sigma_R^2 = 6$ a.u. AND $\sigma_N^2 = 10$ a.u. EACH ROWS RESPECTIVELY FROM THE LEFT TO THE RIGHT CORRESPONDS TO THE NUMBER OF RTs, THE MEAN, MEDIAN, STANDARD DEVIATION, MINIMUM AND MAXIMUM VALUE OF THE 95% UPPER BOUND

RTs number	Spectrum average 95% upper limit				
	Mean	Median	Std	Min	Max
2	112.99	79.45	32.93	48.50	440.60
3	98.41	72.60	35.66	31.70	453.20
4	78.00	51.50	18.30	23.80	260.10
5	90.11	67.95	28.47	19.00	373.40
RTs number	Cross-spectrum 95% upper limit				
	Mean	Median	Std	Min	Max
2	116.49	83.00	27.38	67.90	388.90
3	99.74	79.65	34.54	41.00	443.40
4	76.37	54.10	18.03	28.50	255.80
5	91.87	65.35	28.98	22.20	380.20
RTs number	s.a/c-s 95% upper limit				
	Mean	Median	Std	Min	Max
2	0.97	0.90	0.12	0.71	2.21
3	0.98	0.94	8.13×10^{-2}	0.74	1.79
4	1.02	0.98	4.86×10^{-2}	0.74	1.50
5	0.97	0.96	3.73×10^{-2}	0.78	1.34

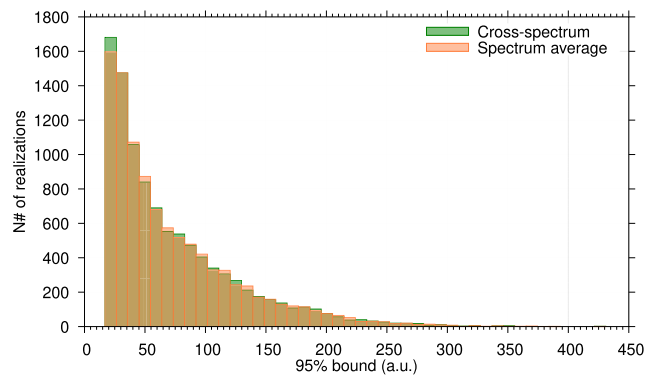


Fig. 5. Histogram comparison of 95% upper bound between the c-s and s.a for 10000 realizations. The parameters are set for five RTs, $\sigma_R^2 = 6$ a.u. and $\sigma_N^2 = 10$ a.u.

Let us now compare the s.a and c-s 95% upper limit over 100 simulations as shown in Table III for the sought signal-level set to 6 a.u. and a noise level equal to 10 a.u. for each RT. The 95% upper limit is given respectively for, from the top of the Table to the bottom, the spectrum average, the cross-spectrum, and the ratio of the 95% bound of s.a over c-s. The mean and median are decreasing when the number

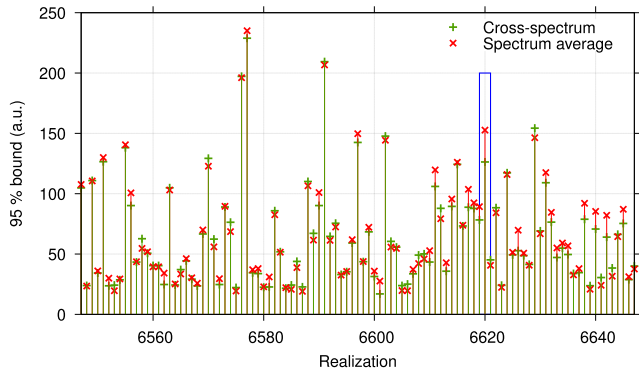


Fig. 6. Set of 100 realizations for five RTs of 95% bounds for cross-spectrum (green +) and spectrum average (red x) where $\sigma_R^2 = 6$ a.u. and $\sigma_N^2 = 10$ a.u.

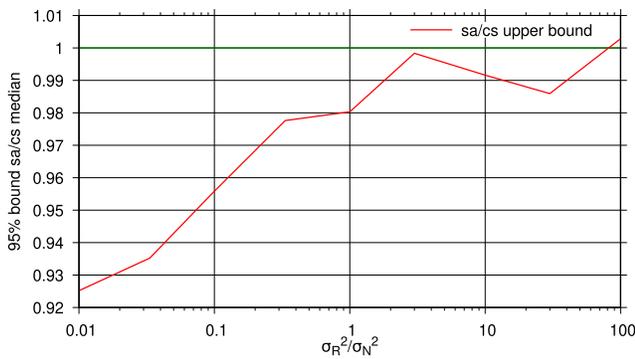


Fig. 7. Evolution of the 95% upper bound median of the s.a over c-s ratio obtained for 1000 realizations depending on the signal-to-noise level ratio. The parameters are set for 5 RTs and $\sigma_N^2 = 1$ a.u. The red curve corresponds to the sa/cs upper bound and the green curve indicates when both s.a and c-s have the same upper bound in median.

of RTs is increasing. However, for four RTs the results are much more lower but it is just an artifact of “luck.” Indeed the maximum value is 1.4 times lower than for five RTs and the standard deviation (std) is also very much more lower. The sample size can have a significant effect on the values obtained but is necessary to have a good precision with a reasonable computation time. However, the minimum value of the 95% bound obtained for both methods permits to override this randomness. Indeed when the cross-spectrum estimate is negative or the spectrum average estimate tends toward zero it leads to the smallest 95% bound. Whereas the maximum 95% bound obtainable for a reasonable amount of simulations can “wriggle” a lot as the tail of the posterior PDF is very long especially with higher noise level than signal level which is of interest. The minimum value of the upper bound decreases as the number of RTs increases. It seems that the s.a method gives the most stringent confidence interval.

Fig. 5 shows the histogram of the 95% limit with 5 RTs for 10000 realizations, $\sigma_R^2 = 6$ a.u. and $\sigma_N^2 = 10$ a.u. Both histograms exhibit a similar distribution which extend up to high values. However, the first bin corresponding to the lowest 95% bound shows a high number of realizations for the c-s method. This can be explained by a negative

estimate for the cross-spectrum which may corresponds to a spectrum average estimate having a not so small value and so a higher 95% bound. Fig. 6 shows the comparison of the 95% upper limit for the s.a and c-s methods for a window of hundred data among the same set of realizations. The 6620th realization framed by a blue rectangle highlights the fact that the c-s can sometimes be much more stringent than the s.a method. However, in most of the other realizations we notice that the 95% limit is almost the same.

Fig. 7 depict the 95% upper bound median among 1000 simulations with five RTs, for the s.a over c-s ratio depending on the signal-to-noise level ratio (with $\sigma_N^2 = 1$ a.u.). When $\sigma_R^2 \ll \sigma_N^2$ then the s.a seems to be the most stringent most of the time. However when the signal level becomes higher than the noise level, both the s.a and the c-s methods give in median the same 95% limit.

Considering all these observations it is wiser to compute both estimators and use the most restrictive one. Even if most of the time both estimators give a very close upper bound, sometimes the gap is clearly significant.

VI. CONCLUSION

First, we demonstrated that the spectrum average variance is $q/(q-1)$ lower than the cross-spectrum variance for $q \geq 2$.

Second, to assess the confidence interval of the signal level we defined its probability density function knowing the s.a and c-s estimates but also the noise of each instruments (RTs). In addition, a method directly using the statistics of the measurement (KLT) has also been compared. It turns out that the KLT and the s.a methods lead to the exact same PDF of the signal-level σ_R^2 knowing the estimates, so the precision is the same. Furthermore, whereas the cross-spectrum has a well-defined analytic probability density function for two instruments called VT, there is no equivalent for more than two instruments. We proposed then a generalized method based on a numerical integration of the characteristic function product. This method works very well according to the Monte Carlo simulations.

Finally, the efficiency of both estimators, the spectrum average versus the cross-spectrum, is highlighted through the comparison of the 95% Bayesian upper limit. We found a slight advantage for the spectrum average estimator when the noise level is higher than the signal level. However, we showed that sometimes the c-s gives the most stringent confidence interval but above all a little more often than the s.a for the lowest upper limit. Nevertheless, it is the s.a method which gives us the minimum 95% limit reachable. To conclude, it is wiser to compute both estimates and use the most stringent.

APPENDIX

Glossary of Symbols

q	Number of instruments.
$r(t)$	Common signal measured by q RTs (red noise).
$R(f)$	Fourier transform of $r(t)$.
$S_r(f)$	Power spectral density of $r(t)$.
$n_i(t)$	Intrinsic white noise of the i th RT.

$N_i(f)$	Fourier transform of $n_i(t)$.
$S_{n,i}(f)$	Power spectral density of $n_i(t)$.
$x_i(t)$	$x_i(t) = r(t) + n_i(t)$, received at the output of the i th RT.
$X_i(f)$	Fourier transform of $x_i(t)$.
$S_{x,i}(f)$	Power spectral density of $x_i(t)$.
\widehat{S}_{sa}	estimate as in \widehat{S} . Here we consider three estimators
\widehat{S}_{sa}	Spectrum average.
\widehat{S}_{KLT}	Karhunen-Loève transform.
\widehat{S}_{cs}	Cross-spectrum.
σ_R^2	Variance of R in a bandwidth, i.e., the power in one bin of $S(f)$. It takes three different flavors: s.a, KLT or c-s.
$\sigma_{N,i}^2$	Same as above, with the noise of the i th RT.
σ_μ^2	Noise weight factor, inverse of the sum of the inverse of $\sigma_{N,i}^2$.

Variance of the Estimators \widehat{S}_{sa} and \widehat{S}_{cs}

1) **Measurements:** Let us define q instruments measurements X_1, X_2, \dots , and X_q as

$$X_j = N_j + iN'_j + R + iR' \quad (38)$$

where N_j, N'_j are independent Gaussian-centered random variables of variance $\sigma_N^2/2$ and R, R' are independent Gaussian-centered random variables of variance $\sigma_R^2/2$.

2) **Estimators:** The estimator \widehat{S}_{cs} is defined by (10) as

$$\widehat{S}_{cs} = \frac{1}{\binom{q}{2}} \sum_{j=1}^{q-1} \sum_{k=j+1}^q \Re[(N_j + iN'_j + R + iR') \times (N_k - iN'_k + R - iR')]. \quad (39)$$

On the other hand, \widehat{S}_{sa} is defined by (10) as

$$\widehat{S}_{sa} = \left(\sum_j \frac{N_j + qR}{q} \right)^2 + \left(\sum_j \frac{N'_j + qR'}{q} \right)^2. \quad (40)$$

3) **Statistics Reminder:** If A and B are two independent random variables of zero expectation

$$\mathbb{V}[AB] = \mathbb{V}[A]\mathbb{V}[B] \quad (41)$$

according to (a) from [19] where $\mathbb{V}[\cdot]$ stands for the variance of the quantity within the brackets. Moreover, according to the Isserlis' theorem [20]

$$\begin{aligned} \mathbb{V}[A^2] &= \mathbb{E}[A^4] - \{\mathbb{E}[A^2]\}^2 = 3\{\mathbb{E}[A^2]\}^2 - \{\mathbb{E}[A^2]\}^2 \\ &= 2\mathbb{V}^2[A] \end{aligned} \quad (42)$$

where $\mathbb{E}[\cdot]$ stands for the mathematical expectation of the quantity within the brackets. It is also useful to consider the covariances. If A, B, C, D are four Gaussian centered random variable

$$\begin{aligned} \mathbb{E}[ABCD] &= \mathbb{E}[AB] \cdot \mathbb{E}[CD] + \mathbb{E}[ac] \cdot \mathbb{E}[BD] \\ &\quad + \mathbb{E}[AD] \cdot \mathbb{E}[BC]. \end{aligned} \quad (43)$$

If A, B, C, D are 4 independent Gaussian-centered random variables, this can be derived to the following particular cases (Isserlis' theorem [20]):

- 1) $\mathbb{E}[ABCD] = \mathbb{E}[AB] \cdot \mathbb{E}[CD] + \mathbb{E}[ac] \cdot \mathbb{E}[BD] + \mathbb{E}[AD] \cdot \mathbb{E}[BC] = 0$ since each mathematical expectation product $\mathbb{E}[XY]$ is null
- 2) $\mathbb{E}[A^2BC] = \mathbb{E}[A^2] \cdot \mathbb{E}[BC] + 2\mathbb{E}[AB] \cdot \mathbb{E}[ac] = 0$ since the only mathematical expectation which is not null, $\mathbb{E}[A^2]$, is multiplied by $\mathbb{E}[CD] = 0$
- 3) $\mathbb{E}[A^3B] = 3\mathbb{E}[A^2] \cdot \mathbb{E}[BC] = 0$ since $\mathbb{E}[BC] = 0$
- 4) $\mathbb{E}[A^2B^2] = \mathbb{E}[A^2] \cdot \mathbb{E}[B^2] + 2\mathbb{E}[AB] = \mathbb{E}[A^2] \cdot \mathbb{E}[B^2] \neq 0$.
- 5) $\text{Cov}[A^2B^2] = \mathbb{E}[A^2B^2] - \mathbb{E}[A^2] \cdot \mathbb{E}[B^2] = \mathbb{E}[A^2] \cdot \mathbb{E}[B^2] - \mathbb{E}[A^2] \cdot \mathbb{E}[B^2] = 0$.

4) **Variance of \widehat{S}_{cs} :** From (39), it comes

$$\begin{aligned} \widehat{S}_{cs} &= \frac{1}{\binom{q}{2}} \left[\sum_{j=1}^{q-1} \sum_{k=j+1}^q (N_j N_k + N'_j N'_k) \right. \\ &\quad \times (q-1) \sum_{j=1}^q (N_j R + N'_j R') \\ &\quad \left. \times \binom{n}{2} (R^2 + R'^2) \right]. \end{aligned} \quad (44)$$

Then

$$\begin{aligned} \mathbb{V}[\widehat{S}_{cs}] &= \frac{1}{\binom{q}{2}^2} \left[\sum_{j=1}^{q-1} \sum_{k=j+1}^q (\mathbb{V}[N_j N_k] + \mathbb{V}[N'_j N'_k]) \right. \\ &\quad \times (q-1)^2 \sum_{j=1}^q (\mathbb{V}[N_j R] + \mathbb{V}[N'_j R']) \\ &\quad \left. \times \binom{q}{2}^2 (\mathbb{V}[R^2] + \mathbb{V}[R'^2]) \right]. \end{aligned} \quad (45)$$

where all covariance terms are null thanks to Isserlis' theorem. From the properties (41) and (42), it comes

$$\begin{aligned} \mathbb{V}[\widehat{S}_{cs}] &= \frac{1}{\binom{q}{2}^2} \left[\sum_{j=1}^{q-1} \sum_{k=j+1}^q (\mathbb{V}[N_j]\mathbb{V}[N_k] + \mathbb{V}[N'_j]\mathbb{V}[N'_k]) \right. \\ &\quad \times (q-1)^2 \sum_{j=1}^q (\mathbb{V}[N_j]\mathbb{V}[R] + \mathbb{V}[N'_j]\mathbb{V}[R']) \\ &\quad \left. \times \binom{q}{2}^2 (2\mathbb{V}^2[R] + 2\mathbb{V}^2[R']) \right]. \end{aligned} \quad (46)$$

According to the binomial formula

$$\binom{q}{2} = \frac{q!}{2!(q-2)!} = \frac{q(q-1)}{2}. \quad (47)$$

Therefore

$$\begin{aligned} \mathbb{V}[\widehat{S}_{cs}] &= \frac{1}{\binom{q}{2}^2} \left[2 \binom{q}{2} \frac{\sigma_N^4}{4} + 2q(q-1)^2 \frac{\sigma_N^2 \sigma_R^2}{4} + 4 \binom{q}{2}^2 \frac{\sigma_R^4}{4} \right] \\ &= \frac{1}{q(q-1)} \sigma_N^4 + \frac{2}{q} \sigma_N^2 \sigma_R^2 + \sigma_R^4. \end{aligned} \quad (48)$$

5) *Variance of \widehat{S}_{sa}* : From (40), it comes

$$\widehat{S}_{sa} = \frac{1}{q^2} \left[\sum_{j=1}^q (N_j^2 + N_j'^2) + q^2(R^2 + R'^2) + 2 \sum_{j=1}^{q-1} \sum_{k=j+1}^q (N_j N_k + N_j' N_k') + 2q \sum_{j=1}^q (N_j R + N_j' R') \right]. \quad (49)$$

Then

$$\mathbb{V}[\widehat{S}_{sa}] = \frac{1}{q^4} \left[\sum_{j=1}^q (\mathbb{V}[N_j^2] + \mathbb{V}[N_j'^2]) + q^4(\mathbb{V}[R^2] + \mathbb{V}[R'^2]) + 4 \sum_{j=1}^{q-1} \sum_{k=j+1}^q (\mathbb{V}[N_j N_k] + \mathbb{V}[N_j' N_k']) + 4q^2 \sum_{j=1}^q (\mathbb{V}[N_j R] + \mathbb{V}[N_j' R']) \right] \quad (50)$$

where all covariance terms are null thanks to Isserlis' theorem. From the properties (41) and (42), it comes

$$\mathbb{V}[\widehat{S}_{sa}] = \frac{1}{q^4} \left[\sum_{j=1}^q (2\mathbb{V}^2[N_j] + 2\mathbb{V}^2[N_j']) + q^4(2\mathbb{V}^2[R] + 2\mathbb{V}^2[R']) + 4 \sum_{j=1}^{q-1} \sum_{k=j+1}^q (\mathbb{V}[N_j]\mathbb{V}[N_k] + \mathbb{V}[N_j']\mathbb{V}[N_k']) + 4q^2 \sum_{j=1}^q (\mathbb{V}[N_j]\mathbb{V}[R] + \mathbb{V}[N_j']\mathbb{V}[R']) \right]. \quad (51)$$

Therefore

$$\begin{aligned} \mathbb{V}[\widehat{S}_{sa}] &= \frac{1}{q^4} \left[4q \frac{\sigma_N^4}{4} + 4q^4 \frac{\sigma_R^4}{4} + 8 \binom{q}{2} \frac{\sigma_N^4}{4} + 8q^3 \frac{\sigma_N^2 \sigma_R^2}{4} \right] \\ &= \frac{1}{q^2} \sigma_N^4 + \frac{2}{q} \sigma_N^2 \sigma_R^2 + \sigma_R^4. \end{aligned} \quad (52)$$

6) *Variance Ratios*: Let us compare the cross-spectrum and spectrum average estimates variances for limit signal-to-noise ratio values.

If $\sigma_R^2 \ll \sigma_N^2$

$$\mathbb{V}[\widehat{S}_{cs}] \approx \frac{1}{q(q-1)} \sigma_N^4 \quad \text{and} \quad \mathbb{V}[\widehat{S}_{sa}] \approx \frac{1}{q^2} \sigma_N^4. \quad (53)$$

Consequently

$$\mathbb{V}[\widehat{S}_{cs}] \approx \frac{q}{q-1} \mathbb{V}[\widehat{S}_{sa}]. \quad (54)$$

If $\sigma_N^2 \ll \sigma_R^2$

$$\mathbb{V}[\widehat{S}_{cs}] \approx \sigma_R^4 \quad \text{and} \quad \mathbb{V}[\widehat{S}_{sa}] \approx \sigma_R^4. \quad (55)$$

Consequently

$$\mathbb{V}[\widehat{S}_{cs}] \approx \mathbb{V}[\widehat{S}_{sa}]. \quad (56)$$

REFERENCES

- [1] L. A. Rawley, J. H. Taylor, M. M. Davis, and D. W. Allan, "Millisecond pulsar PSR 1937+21: A highly stable clock," *Science*, vol. 238, no. 4828, pp. 761–765, Nov. 1987.
- [2] J. H. Taylor, Jr., "Millisecond pulsars: Nature's most stable clocks," *Proc. IEEE*, vol. 79, no. 7, pp. 1054–1062, Jul. 1991.
- [3] J. G. Hartnett and A. N. Luiten, "Colloquium: Comparison of astrophysical and terrestrial frequency standards," *Rev. Modern Phys.*, vol. 83, no. 1, pp. 1–9, Jan. 2011.
- [4] R. N. Manchester, "Millisecond pulsars, their evolution and applications," *J. Astrophys. Astron.*, vol. 38, no. 3, pp. 1–18, Sep. 2017.
- [5] J. E. Hansen and M. Sato, "Paleoclimate implications for human-made climate change," in *Climate Change*, A. Berger, F. Mesinger, and D. Sijacki, Eds. Vienna, Austria: Springer, 2012, pp. 21–47.
- [6] A. Nothnagel. (Nov. 2021). *Elements of Geodetic and Astrometric Very Long Baseline Interferometry*. [Online]. Available: https://www.vlbi.at/data/publications/2021_Nothnagel_Elements_of_VLBI_20211102.pdf
- [7] C. Massimo, G. A. Costanzo, and C. E. Calosso, "6/12-channel synchronous digital phasemeter for ultrastable signal characterization and use," in *Proc. Joint Conf. IEEE Int. Freq. Control Symp. Eur. Freq. Time Forum*, Apr. 2015, pp. 681–683.
- [8] V. Palenskis and K. Maknys, "Nature of low-frequency noise in homogeneous semiconductors," *Sci. Rep.*, vol. 5, no. 1, pp. 1–7, Dec. 2015.
- [9] M. E. Tiuri, "Radio-telescope receivers," in *Radio Astronomy*, J. D. Kraus, Ed. New York, NY, USA: McGraw-Hill, 1966, ch. 7.
- [10] A. Baudiquez, E. Lantz, E. Rubiola, and F. Vernotte, "Cross-spectrum measurement statistics: Uncertainties and detection limit," *IEEE Trans. Ultrason., Ferroelectr., Freq. Control*, vol. 67, no. 11, pp. 2461–2470, Nov. 2020.
- [11] C. G. Bassa *et al.*, "Leap: The large European array for pulsars," *Month. Not. Roy. Astronom. Soc.*, vol. 456, no. 2, pp. 2196–2209, Dec. 2015.
- [12] J. P. W. Verbiest, S. Osłowski, and S. Burke-Spolaor, "Pulsar timing array experiments," in *Handbook of Gravitational Wave Astronomy*, C. Bambi, S. Katsanevas, and K. D. Kokkotas, Eds. Singapore: Springer, 2020, pp. 1–42, doi: [10.1007/978-981-15-4702-7_4-1](https://doi.org/10.1007/978-981-15-4702-7_4-1).
- [13] B. Goncharov *et al.*, "On the evidence for a common-spectrum process in the search for the nanohertz gravitational-wave background with the parkes pulsar timing array," *Astrophys. J. Lett.*, vol. 917, no. 2, p. L19, Aug. 2021.
- [14] S. Chen, F. Vernotte, and E. Rubiola, "Applying clock comparison methods to pulsar timing observations," *Monthly Notices Roy. Astronomical Soc.*, vol. 503, no. 3, pp. 4496–4507, May 2021.
- [15] N. J. Kasdin, "Discrete simulation of colored noise and stochastic processes and $1/f^n$ power law noise generation," *Proc. IEEE*, vol. 83, no. 5, pp. 802–827, May 1995.
- [16] J. Hartung, G. Knapp, and B. K. Sinha, *Statistical Meta-Analysis with Applications*. Hoboken, NJ, USA: Wiley, 2008.
- [17] E. Lantz *et al.*, "KLTS: A rigorous method to compute the confidence intervals for the three-cornered hat and for Gros Lambert covariance," *IEEE Trans. Ultrason., Ferroelectr., Freq. Control*, vol. 66, no. 12, pp. 1942–1949, Dec. 2019.
- [18] M. P. McHugh, G. Zalamansky, F. Vernotte, and E. Lantz, "Pulsar timing and the upper limits on a gravitational wave background: A Bayesian approach," *Phys. Rev. D, Part. Fields*, vol. 54, no. 10, pp. 5993–6000, Nov. 1996.
- [19] H. A. R. Barnett, "The variance of the product of two independent variables and its application to an investigation based on sample data," *J. Inst. Actuaries*, vol. 81, no. 2, p. 190, 1955.
- [20] L. Isserlis, "On a formula for the product-moment coefficient of any order of a normal frequency distribution in any number of variables," *Biometrika*, vol. 12, nos. 1–2, pp. 134–139, 1918.